COMBINED REMOVAL OF DIESEL SOOT PARTICULATES AND NOx OVER CeO_2-ZrO_2 MIXED OXIDES.

I. Atribak, A. Bueno-López*, and A. García-García.

Department of Inorganic Chemistry, University of Alicante,
Ap.99 E-03080, Alicante, Spain.
(atribak@ua.es, agus@ua.es, a.garcia@ua.es)

Abstract

CeO_2 and Ce-Zr mixed oxides with different Ce:Zr ratio have been prepared, characterised by Raman spectroscopy, XRD, TEM, N_2 adsorption at -196ºC and H_2-TPR, and tested for soot oxidation under NO_x/O_2. Among the different mixed oxides, $Ce_{0.76}Zr_{0.24}O_2$ provided the best results. $Ce_{0.76}Zr_{0.24}O_2$ presents a higher activity than pure CeO_2 for soot oxidation by NO_x/O_2 when both catalysts are calcined at 500ºC (soot oxidation rates at 500ºC are 14.9 and 11.4 $\mu g_{soot}/s$, respectively), and the catalytic activity of CeO_2 decays significantly with calcination temperature (from 500 to 1000ºC) while $Ce_{0.76}Zr_{0.24}O_2$ presents enhanced thermal stability at temperatures as high as 1000ºC. In addition, $Ce_{0.76}Zr_{0.24}O_2$ catalyses more efficiently than CeO_2 the reduction of NO_x by soot around 500ºC, therefore contributing to the decrease of the NO_x emission level. The catalytic activity of CeO_2 and $Ce_{0.76}Zr_{0.24}O_2$ for soot oxidation by NO_x/O_2 depends on the textural properties (BET area; crystallite size), but other properties of the oxides, like redox behaviour and/or enhanced lattice oxygen mobility, also play a significant role.

Keywords: catalysed soot oxidation; ceria; Ce-Zr mixed oxide; solid solution; soot; NO_x; Diesel pollution control;

* Corresponding author
Tel.: +34 965 90 34 00 (2226)
Fax: +34 965 90 34 54

1.- Introduction.

Ceria is an important material in the framework of the three-way catalysts (TWCs) which are used in gasoline automobile catalytic converters for the treatment of exhaust gases [1, 2]. One of the key functions of this material is the ability of cerium to switch between the Ce^{4+} and Ce^{3+} oxidation states and to incorporate more or less oxygen into their crystal structure depending on various parameters such as the gaseous atmosphere with which they are in contact, temperature and pressure [3]. Therefore, early on, ceria was given a main role as oxygen storage component in order to extend the three-way window on the lean side of stoichiometry by acting as a sink for gas-phase oxygen during rich-to-lean transients in air-to-fuel ratio [1-3]. On the other hand, the oxygen storage component could also promote oxidation of reductants, like CO, during lean-to-rich transients [3]. The TWCs formulation has undergone significant advances during the past 20 years, mainly employing ceria in solid solution with other metal oxides, most notably zirconia [1, 4]. The advanced TWC formulations are capable of much higher temperature operation than their predecessors and have dramatically improved long-term emissions performance [2, 4].

It has been established that addition of zirconium to ceria to form a mixed oxide solution greatly enhances the reducibility of Ce^{4+} in the catalyst material, which has generated considerable interest in the Ce-Zr system [5-8]. The energetics of the Ce^{4+}/Ce^{3+} reduction step and the corresponding formation of oxygen vacancies are likely to be involved [9]. Indeed, it is clear that fundamental solid state properties such as the precise role of structural defects and dopants, the nature of redox reactions to create electronic species (both within the bulk and at the surfaces), as well as the mechanism of oxygen migration, are crucial to the greater understanding of these important materials.

The unique features of oxygen storage capacity have made Ce-Zr binary oxides important in numerous catalytic processes, besides TWCs, also CO oxidation [10], light hydrocarbon combustion [11, 12] and VOC oxidation [13]. The key steps of these reactions are the supply of oxygen by the readily reducible mixed oxide and its re-oxidation by oxygen. The Ce-Zr mixed oxides are better catalysts than bare CeO_2 because the partial substitution of Ce^{4+} (ionic radii = 0.97 Å) with Zr^{4+} (ionic radii = 0.84 Å) leads to the deformation of the lattice, improving its oxygen storage capacity, redox properties and thermal resistance [5-8, 14, 15].

It has been also recently reported [16] the important role of the active oxygen generated by CeO_2 in the catalysed oxidation of soot by O_2, which seems to be of interest for the utilization of this oxide as catalyst for the regeneration of soot traps fitted in the exhaust of Diesel engines [17, 18]. It has been also shown that ceria doped with Zr [19], La [20, 21] or Pr [21] results in more active catalysts for soot oxidation by O_2, but scarce information has been reported regarding soot combustion under NOx/O_2 mixtures catalysed by Ce-Zr mixed oxides.

The catalytic behaviour of CeO_2 for soot oxidation in O_2 is not the same than that in the presence of NOx. In a previous study, the catalytic activity of pure TiO_2, ZrO_2, and CeO_2 for soot oxidation under $NOx+O_2$ mixtures was compared [22], concluding that the best activity of CeO_2 is related to its capacity to accelerate the NO conversion to NO_2 (TiO_2 and ZrO_2 do not catalyse this reaction), NO_2 being much more oxidant than NO and O_2 [23]. Rare earth-doped ceria catalysts (Rare earth = Sm, Y, La or Pr) have been also studied for soot oxidation by NOx/O_2, concluding that La and Pr doping enhances ceria activity and stability, while Sm and Y do not provide such benefit [24, 25].

It has been reported [22] that CeO_2 catalyses the reduction of NOx by soot, removing both Diesel pollutants - soot and NO_x - simultaneously. The simultaneous removal of NOx and soot was previously studied by Pisarello et al. [26] with catalysts containing Co, K and/or Ba supported on MgO, La_2O_3 and CeO_2, concluding that CeO_2 supplies the oxygen necessary for the redox mechanism that takes place during the reaction.

The scope of this paper is to study the catalytic performance of Ce-Zr mixed oxides for the removal of soot under simulated Diesel exhaust conditions in a gas flow containing O_2 and NOx. Special attention is paid to the simultaneous removal of NOx. The catalytic activity of the Ce-Zr mixed oxides is compared with that of pure CeO_2 and the thermal stability of the pure and mixed oxides is studied in detail since the thermal stability is a key requirement for the application of these materials in a real soot trap.

2.- Experimental

2.1. Catalyst preparation

Ce-Zr mixed oxides with different metal ratio were prepared by using a co-precipitation route. The required amounts of $ZrO(NO_3)_2 \cdot 6H_2O$ and/or $Ce(NO_3)_3 \cdot 6H_2O$ (supplied by Aldrich) were dissolved in water and the hydroxides were precipitated by dropping an ammonia solution to keep the pH about 9. The precipitates were dried at 90ºC in air overnight and calcined in air for 3 hours at different temperatures in the range 500-1000ºC. Pure CeO_2 and ZrO_2 were also prepared following the same procedure.

CeO_2 and ZrO_2 pure oxides are denoted by CeO_2-T and ZrO_2-T, respectively, and the Ce-Zr mixed oxides are denoted by $Ce_xZr_{1-x}O_2$-T, (formal composition, $0<x<1$) where x is the molar fraction of CeO_2 in the mixed oxides and T is the calcination temperature.

2.2. Catalytic tests

The catalytic tests were performed in a tubular quartz reactor coupled to specific NDIR-UV gas analysers for CO, CO_2, NO, NO_2 and O_2 monitoring. 20 mg of soot and 80 mg of the selected catalyst were mixed in the so-called *loose contact* conditions [27] and diluted with SiC to avoid pressure drop and favour heat transfer. The gas mixture used contained 500 ppm NOx, 5% O_2 and balance N_2, and the gas flow was fixed at 500 ml/min (GHSV = 30000 h^{-1}).

Two types of experiments were carried out:

i) Temperature Programmed Reactions: the gas mixture was fed to the reactor, which was at room temperature, and then the temperature was increased from room temperature until 700ºC at 10ºC/min.

ii) Isothermal Reactions at 500ºC: the temperature was raised from room temperature until 500ºC, maintaining the soot-catalyst mixture in N_2 flow, and then the N_2 flow was replaced by the reaction gas mixture. These experiments were conducted until total conversion of soot.

The model soot used is a carbon black from Degussa (Printex U), with < 0.1 % ash content, 5 % volatile matter, 92.2 % C, 0.6 % H, 0.2 % N and 0.4 % S.

Soot conversion profiles were determined from CO and CO_2 evolved and the selectivity of the different catalysts towards CO emission was determined with the equation:

$$CO/CO_x\ (\%) = 100 \cdot CO/(CO + CO_2)$$

Blank experiments were performed under the described experimental conditions but without soot, that is, only using catalyst.

2.3. Characterization techniques

The textural properties were determined by multi-point N_2 adsorption at -196°C using an automatic Autosorb-6B (Quantachrome equipment). Data were treated in accordance with the BET method. The samples were previously degassed for 4 hours at 250°C under vacuum.

A JOEL (JEM-2010) microscope was used to obtain TEM images of the catalysts. Few droplets of an ultrasonically dispersed suspension of each catalyst in ethanol were placed in a grid and dried at ambient conditions for TEM characterisation.

Raman spectra of the catalysts were recorded in a Bruker RFS 100/S Fourier Transform Raman Spectrometer with a variable power Nd:YAG laser source (1064 nm). 64 scans at 85 mW laser power (70 mW on the sample) were recorded and no heating of the sample was observed under these conditions.

X-ray difractograms of the catalysts were recorded in a Bruker D8 advance diffractometer, using CuK_α radiation. Spectra were registered between 10 and 80º (2θ) with a step of 0.02º and a time per step of 3 seconds. The average crystal size (D) of the catalysts was determined using the equations of Scherrer and Williamson-Hall:

$$D = \frac{K \cdot \lambda}{\beta \cdot \cos\theta}$$ Scherrer's equation

where λ is the wavelength of the radiation used (λ = 0.15418 nm for CuK_α), β is the full width at half maximum of the diffraction peak considered (111), K is a shape factor, which is taken as 0.9 (1 being a perfect sphere) and θ is the diffraction angle at which the peak appears.

The estimation of crystal size of doped oxides presents some problems, because the introduction of foreign cations within the lattice deforms the structure and affects the β values. The Williamson–Hall's equation separates the effects of size and strain in the crystals, and is more convenient for the estimation of crystal size of mixed oxides:

$$\beta_{Total} = \beta_{Size} + \beta_{Strain} = \frac{0.9 \cdot \lambda}{D \cdot \cos\theta} + \frac{4 \cdot (\Delta d) \cdot \sin\theta}{d \cdot \cos\theta} \qquad \text{Williamson–Hall's equation}$$

where β_{Total} is the full width half maximum of the XRD peak and Δd is the difference of the d spacing corresponding to a typical peak. A plot of $\beta_{Total} \cdot \cos\theta$ against $4 \cdot \sin\theta$ yields the average crystal size from the intercept value. In spite of the improvement introduced by the Williamson–Hall's equation with regard to the Scherrer's equation, the crystal sizes estimated for the Ce-Zr mixed oxides prepared in this study must be considered as semi-quantitative values, since some of the data obtained are not fully consistent with the BET areas estimated by N_2 adsorption.

The redox behaviour of the catalysts was examined by H_2-Temperature-Programmed Reduction (H_2-TPR) in a Micromeritics Pulse ChemiSorb 2705 device consisting of a tubular quartz reactor coupled to a TCD detector in order to monitor H_2 consumption. The reducing gas used was 5% H_2 in He. The temperature range explored was from room temperature to 900°C, and the heating rate 10°C/min.

3. Results and discussion.

3.1 Temperature programmed reactions: Soot oxidation.

On Figure 1, the catalytic activity of two series of Ce-Zr mixed oxides, calcined at 500 and 1000 ºC respectively, is compared. The temperature required to convert 50% of soot (T50%) in each experiment is plotted as a function of the Zr molar fraction of the

catalysts used. The T50% temperature for the uncatalysed reaction was 606 ºC under the experimental conditions used, and most of the samples decreased this temperature. Among the catalysts calcined at 500ºC, CeO_2-500 and $Ce_{0.76}Zr_{0.24}O_2$-500 presented the best performance, and increasing the Zr loading above this molar fraction has a negative effect on the activity due to the lower amount of Ce available. This is consistent with the fact that the couple $Ce^{3+/4+}$ is the responsible of the catalytic activity for soot oxidation of CeO_2-based catalysts. The same activity trend has been reported [19] for $Ce_xZr_{1-x}O_2$-catalysed soot combustion in air ($0 \leq x \leq 1.0$ composition; catalysts calcined at 500ºC; soot and catalyst in tight contact), where the highest activity was obtained with cerium-rich mixtures (with x = 1.0 and x = 0.75). The arguments provided [19] to explain these results were: i) cerium-rich samples present higher availability of surface Ce^{4+} sites and, ii) the better ability of these materials (solid solutions) to donate its oxygen for soot oxidation. The highest catalytic activity of $Ce_xZr_{1-x}O_2$ mixed oxides with $x \sim 0.75$, in comparison with higher zirconium loading, has been also reported for the selective catalytic reduction of NOx by hydrocarbons [28].

The activity of the catalysts decreased when they were calcined at 1000 ºC (Figure 1), and the degree of thermal deactivation depends on their composition: (i) pure CeO_2 and pure ZrO_2 became inactive when calcined at 1000ºC, (ii) $Ce_{0.76}Zr_{0.24}O_2$ suffered a partial decrease in activity after calcination at 1000ºC, and (iii) the Ce-Zr mixtures with Zr molar fraction higher than 0.24 calcined at 1000ºC maintained the poor activity of the counterpart catalysts calcined at 500ºC. The thermal stability of CeO_2 is a critical point for its application in catalysis, as occurred in TWCs where the low stability of the pure CeO_2 used in early formulations obligated to develop advanced CeO_2-based materials with enhanced

thermal resistance [2]. The effect of foreign cation doping on the thermal stability of CeO_2 was extensively investigated by Pijolat et al. [29], concluding that, among the different cations investigated (Th^{4+}, Zr^{4+}, Si^{4+}, La^{3+}, Y^{3+}, Sc^{3+}, Al^{3+}, Ca^{2+}, and Mg^{2+}), those with ionic radii smaller than that of Ce^{4+} effectively stabilised the CeO_2 against sintering. This observation is consistent with the improved thermal resistance of $Ce_{0.76}Zr_{0.24}O_2$ in comparison to pure CeO_2.

An additional feature of the soot oxidation catalysts that must be analysed together with the decrease in soot oxidation temperature is the production of CO_2 and/or CO as soot gasification product, CO_2 being the desired gas product due to the high toxicity of CO. A general feature of carbon combustion reactions is that the production of CO increases and the production of CO_2 diminishes with temperature. Therefore, on one hand, whether a catalyst decreases the soot combustion temperature, CO_2 formation is favoured and, on the other hand, CeO_2-based catalysts are effective to catalyse the oxidation of CO to CO_2 [2]. Both properties of the catalysts determine the amount of CO and CO_2 yielded during the catalysed soot oxidation reactions.

On Figure 2, the percentage of CO evolved during the experiments performed with the series of catalysts calcined at 500 and 1000ºC is included. The uncatalysed reaction yields 65% CO, and all the catalysts decreased this value with the only exception of CeO_2-1000. The best results were obtained with CeO_2-500 and with Ce-Zr mixtures with Zr molar fraction equal or lower than 0.46. The calcination temperature of the Ce-Zr mixtures had a minor effect on CO selectivity.

As a summary of the results included on Figures 1 and 2, it can be concluded that the best formulation obtained among those tested is $Ce_{0.76}Zr_{0.24}O_2$. This material has the same activity and selectivity for CO_2 formation than pure CeO_2 when both catalysts are

calcined at 500ºC, but shows enhanced thermal stability, maintaining part of its activity for soot oxidation and selectivity for CO_2 formation after calcinations at a temperature as high as 1000ºC. This conclusion is in agreement with that reached by Aneggi et al. [19] for CeO_2- and $Ce_{0.75}Zr_{0.25}O_2$-catalysed soot combustion in air (with catalysts calcined at 500 and 800ºC), who concluded that the main difference between pure ceria and cerium–zirconium solid solution is related to the stability after calcination.

The effect of calcination temperature on the catalytic activity of CeO_2, ZrO_2 and $Ce_{0.76}Zr_{0.24}O_2$ was studied in more detail within the range of 500-1000ºC, and the results obtained corresponding to activity and selectivity towards CO_2 formation are compiled on Figures 3 and 4, respectively. In all the series of catalysts, the catalytic activity for soot oxidation (Figure 3) decreases with calcination temperature. As expected, ZrO_2 presents very poor activity, regardless the calcination temperature [22]. The activity of CeO_2 and $Ce_{0.76}Zr_{0.24}O_2$ is similar when catalysts are calcined at 500ºC but not at higher calcination temperatures, $Ce_{0.76}Zr_{0.24}O_2$ catalysts being, as a general trend, more active than their counterpart CeO_2 catalysts. The activity of CeO_2 decreases quite monotonically from 500 to 1000ºC, CeO_2-1000 being not active at all. On the contrary, the activity of $Ce_{0.76}Zr_{0.24}O_2$ for soot oxidation suffers a certain decrease between 500 and 600 ºC (T50% increases from 521 to 543ºC, respectively) but is not further modified significantly until 900ºC, indicating very high thermal stability within the range 600-900ºC. The activity of $Ce_{0.76}Zr_{0.24}O_2$ only suffered a further decrease between 900 and 1000ºC, but it still maintains part of its activity.

The effect of calcination temperature on the selectivity towards CO_2 formation depends significantly on the catalyst formulation (Figure 4). Regardless the calcination temperature, $Ce_{0.76}Zr_{0.24}O_2$ yields a low CO percentage (13±6 %) and ZrO_2 a high CO

percentage (53±12 %). CO formation during CeO_2-catalysed soot oxidation suffers a little increase with catalysts calcined between 500 and 600ºC but raises drastically between 600 and 800ºC, almost reaching at this temperature the CO percentage yielded during the uncatalysed reaction. These results confirm that, among the different formulations studied, $Ce_{0.76}Zr_{0.24}O_2$ is the best one considering its activity for soot oxidation, high thermal stability and high selectivity towards CO_2 formation as soot oxidation product.

3.2. Temperature programmed reactions: NO_x elimination.

The elimination of NOx during the Temperature Programmed Reactions also depended on the catalyst used, as observed on Figure 5a for catalysts calcined at 500ºC. This type of profiles was previously studied in detail for pure CeO_2 catalysts [22]. Considering, as an example, the NOx elimination profile obtained with $Ce_{0.76}Zr_{0.24}O_2$ (see Figure 5a), three different processes can be distinguished between 225 and 700ºC, that is, the maximum NOx elimination level is reached at 400ºC, and two shoulders appear at higher temperatures, around 500 and 600 ºC, respectively. This profile suggests that three different NOx elimination pathways are taking place. The shape of the NOx elimination curves depends on the catalyst used, in other words, the relative importance of each NOx elimination pathway is different for each catalyst. The NO_x elimination profiles are explained as follows:

- NOx elimination around 400ºC and lower temperatures: the elimination of NOx is mainly attributed to NOx chemisorption on the catalysts, as supported by the blank experiments (without soot) included on Figure 6a. NOx chemisorption on Ce-Zr mixtures (Figure 5a) around 400ºC decreases by increasing the Zr molar fraction, since

NOx chemisorption occurs on Ce but not on Zr [22]. The NOx elimination levels reached at 400ºC by $Ce_{0.76}Zr_{0.24}O_2$-500 and CeO_2-500 (Figure 5a) are slightly different, while the NOx chemisorption in both catalysts observed in blank experiments (Figure 6a) is the same. This suggests a certain contribution of another NOx elimination pathway (NOx reduction by soot), in addition to NOx chemisorption.

- NOx elimination around 500ºC: the elimination of NOx around this temperature is partially attributed to the catalysed soot-NOx reaction, and NOx is consumed due to reduction by soot. This is the most interesting NOx elimination pathway, since allows the simultaneous abatement of NOx and soot by reaction of both pollutants to each other. The formation of N_2O, as reaction product, was not detected in additional experiments followed by gas chromatography [22]. O_2 is also converted around 500ºC due to soot combustion, as observed on Figure 5b. As mentioned in the previous section, the catalytic activity for soot oxidation of the series of catalysts calcined at 500ºC decreases when the Zr molar fraction increases (Figure 1), $Ce_{0.76}Zr_{0.24}O_2$-500 being the most active Ce-Zr mixture.
- NO_x elimination around 600ºC: The elimination of NO_x around this temperature is mainly attributed to the uncatalysed soot-NO_x reaction, occurring along with the reaction soot-O_2 (see Figure 5b). As observed on Figure 5a, this is the only NOx elimination pathway for the least active catalysts (ZrO_2-500, $Ce_{0.16}Zr_{0.84}O_2$-500, and $Ce_{0.34}Zr_{0.66}O_2$-500).

A key factor influencing the catalysed soot oxidation reactions in the presence of NOx is the NO_2 production by the different catalysts. On Figure 6b, the NO_2 percentage (on the basis of NO+NO_2) is plotted as a function of temperature for blank experiments. Above 275ºC, $Ce_{0.76}Zr_{0.24}O_2$-500 and CeO_2-500 catalyse the oxidation of NO to NO_2, reaching a

maximum NO_2 level corresponding to the thermodynamic equilibrium at 450ºC, and decreasing at higher temperature following thermodynamics. On the contrary, the catalysts calcined at 1000ºC are not effective to convert NO into NO_2, which is consistent with the lower activity of the samples $Ce_{0.76}Zr_{0.24}O_2$-1000 and CeO_2-1000 for soot oxidation in comparison to the counterpart samples calcined at 500ºC. It is well established [30] that the catalytic activity for soot oxidation of ceria-based catalysts under NOx mixtures is related to their ability to accelerate NO_2 production, NO_2 being more oxidant than NO and O_2.

The effect of calcination temperature of CeO_2 and $Ce_{0.76}Zr_{0.24}O_2$ on their NOx elimination capacity was also studied, and the curves obtained during the corresponding Temperature Programmed Reactions are included on Figures 7a and 7b, respectively. As shown on Figure 7a, the amount of NOx removed below 500ºC is seen decreased with calcination temperature, existing a dramatic decrease from CeO_2-600 to CeO_2-700. The removal of NO_x through the uncatalysed reaction (around 600ºC) is the main NOx elimination pathway for CeO_2 calcined at 800°C and higher temperatures.

The behaviour of $Ce_{0.76}Zr_{0.24}O_2$-series (Figure 7b) is different to that of CeO_2-series (Figure 7a). $Ce_{0.76}Zr_{0.24}O_2$ suffers a gradual decrease in their NOx removal capacity and only the sample $Ce_{0.76}Zr_{0.24}O_2$-1000 exhibits a NOx profile ascribed only to the uncatalysed NOx-soot reaction. Once more, NOx elimination profiles allow concluding that $Ce_{0.76}Zr_{0.24}O_2$ is the best formulation among those studied, since it presents the best performance among the different catalysts tested and shows enhanced thermal stability with regard to bare CeO_2.

3.3 Isothermal reactions at 500ºC.

As described in the previous sections, the results of the temperature programmed reactions indicated that some of the catalysts tested are able to promote the soot-NOx reaction around 500ºC, therefore allowing the simultaneous removal of both NOx and soot. Considering the best performance of $Ce_{0.76}Zr_{0.24}O_2$, its catalytic activity has been tested under isothermal conditions at 500ºC, and it has been compared with that of bare CeO_2. In both cases, catalysts calcined at 500 and 1000ºC have been tested. The soot oxidation rates, expressed per gram of soot remaining in the reactor, are included on Figure 8a and the corresponding NOx elimination profiles on Figure 8b. Additionally, the average soot oxidation rates estimated from isothermal experiments at 500ºC are compiled on Table 1 as well as the percentage of CO evolved during the experiments and the time required for 75% soot conversion into $CO+CO_2$. It is worth mentioning that the uncatalysed soot oxidation at 500ºC did not take place under these experimental conditions.

$Ce_{0.76}Zr_{0.24}O_2$-500 is the most active catalyst for soot oxidation (Figure 8a) and NO_x reduction (Figure 8b). The soot oxidation rate during the $Ce_{0.76}Zr_{0.24}O_2$-500-catalysed experiment rose with soot conversion until about 25 % of conversion approximately, which can be explained by an increase of the number of actives sites for oxygen chemisorption on the soot surface as a consequence of its progressive oxidation [31, 32]. After a certain conversion, the steady state is reached and a constant rate is maintained. As shown on Table 1, the main reaction product is CO_2, mainly for catalysts calcined at 500°C, with a very low CO emission (according to TPR results). The reduction of NOx (Figure 8b) decreased progressively with the soot conversion, as expected since less reductant is available, and NO_x elimination was null after about 75% soot conversion. However, a low amount of NOx was further eliminated once soot is about consumed, and the NO_x

elimination profiles slightly rose at the end of the experiment. This phenomenon was attributed to the chemisorption of NOx on the catalyst [22]. If soot is available (in Figure 8, below 75% soot conversion for $Ce_{0.76}Zr_{0.24}O_2$-500) the reaction of NOx (mainly NO_2) with soot is preferable to the storage of NO_x on the catalyst, but once soot is not available (above 75% soot conversion), NOx chemisorption on the catalyst takes place being the only possible NO_x elimination pathway.

The calcination temperature of the catalyst diminishes their activity and the soot oxidation rate (Figure 8a) in steady state conditions is about 3 times lower with the catalyst $Ce_{0.76}Zr_{0.24}O_2$-1000 than with $Ce_{0.76}Zr_{0.24}O_2$-500. Under our experimental conditions, 75% of the soot used in the experiments was burnt off after 19 and 62 minutes with $Ce_{0.76}Zr_{0.24}O_2$-500 and $Ce_{0.76}Zr_{0.24}O_2$-1000, respectively. The practical implication of this result is that the regeneration of a DPF loaded with $Ce_{0.76}Zr_{0.24}O_2$-1000 would take about 3 times longer that the regeneration of the same filter loaded with $Ce_{0.76}Zr_{0.24}O_2$-500. The activity of CeO_2-500 also decreased after calcinations at 1000ºC, but in this case the effect of the calcinations temperature was drastic. 172 minutes were required by CeO_2-1000 to convert 75% of the soot used in the experiment while 24 minutes were required by CeO_2-500. Since in a real filter thermal aging of the catalyst can occur, thermally stable active phases are required and $Ce_{0.76}Zr_{0.24}O_2$ is preferable to pure CeO_2. In addition, the activity of CeO_2-500 for soot oxidation and NOx reduction under isothermal conditions at 500ºC is lower than that of $Ce_{0.76}Zr_{0.24}O_2$-500 (Figure 8). These differences were not detected in the transient conditions of the Temperature Programmed Reactions (Figures 1 and 3), evidencing the importance of performing experiments under isothermal conditions, which also provide a more realistic picture of the catalytic behaviour under real conditions.

3.4. Study of the catalytic activity decay due to thermal aging.

The thermal deactivation of CeO_2 and $Ce_{0.76}Zr_{0.24}O_2$ has been studied, and their BET surface areas are represented as a function of the calcination temperature on Figure 9.

The BET surface areas of the samples calcined at 500ºC are about the same value (~65 m^2/g), and the surface areas of all the oxides decrease significantly with calcination temperature. $Ce_{0.76}Zr_{0.24}O_2$ presents much better thermal resistance than pure CeO_2 due to the stabilizing role of Zr. In this type of mixed oxides, the BET value is related to the external surface area of the particles, and high surface area means small particle size and vice versa. The TEM pictures included on Figure 10 are in agreement with this argument and also the crystal sizes determined from XRD by Scherrer and Williamson Hall's equations (Table 2). CeO_2-500 and $Ce_{0.76}Zr_{0.24}O_2$-500 (Figures 10a and 10c, respectively) appear in TEM pictures as a quite homogeneous agglomeration of small particles with a particle size around 10-20 nm in both cases, which is consistent with the crystal sizes determined from the Williamson Hall's equations (22 and 21 nm, respectively). After calcination at 1000ºC, CeO_2 particles grow due to thermal sintering forming particles larger than 100 nm (Figure 10 b) while $Ce_{0.76}Zr_{0.24}O_2$-1000 maintains smaller sizes of around 20-30 nm (Figure 10 d). On this line, the Williamson Hall's equation (Table 2) estimates crystal sizes of 107 and 65 nm for CeO_2-1000 and $Ce_{0.76}Zr_{0.24}O_2$-1000, respectively.

The structural characterization of CeO_2 and $Ce_{0.76}Zr_{0.24}O_2$ samples was carried out by XRD and Raman spectroscopy (Figures 11 and 12 respectively). All the diffractograms included on Figures 11a and 11b contain the main reflections typical of a fluorite-structured material with a fcc unit cell at 28.5, 33.1, 47.6, and 56.5 º, corresponding to the (111),

(200), (220) and (311) planes [33]. Evidences of phase segregation were not observed by XRD for the Ce-Zr mixed oxide (Figure 11b), since ZrO_2 characteristic peaks did not appear. However, a certain degree of inhomogeneous distribution of cerium and zirconium cannot be ruled out, as it will be next discussed in the context of H_2-TPR characterization.

Zr incorporation into the fluorite structure of CeO_2 caused the lattice deformation, and considering a same calcination temperature, the intensity of the CeO_2 peaks is higher than that of the counterpart $Ce_{0.76}Zr_{0.24}O_2$ mixed oxide. This is a consequence of the better arrangement of the atoms into the framework of pure CeO_2 and to the decrease of the number of lattice defects. The effect of calcination temperature is clearly envisaged on Figure 11a. As calcination temperature increases the peaks of CeO_2 become narrower. This is related to an increase in crystal size, which is consistent with BET and TEM characterization, and also with the negative effect of temperature in the catalytic activity of CeO_2. The same effect of temperature is observed in the patterns included on Figure 11b but in a lower extent, in agreement with the higher thermal stability of the Ce-Zr mixed oxide.

Raman characterization supports the conclusions of XRD. All the CeO_2 and $Ce_{0.76}Zr_{0.24}O_2$ samples (Figures 12a and 12b) present the typical structure of CeO_2 with the main band at 460 cm^{-1} attributed to the only allowed Raman mode (F_{2g}) of a fluorite-type structure [34, 35]. The Raman spectra of these fluorite-type oxide structures are dominated by oxygen lattice vibrations and are sensitive to the crystalline symmetry [36]. The presence of Zr^{4+} into the CeO_2 lattice deforms the structure and the intensity of the fluorite-characteristic peak decreases significantly, as deduced by comparison of Figure 12a with Figure 12b. It has been reported that this deformation favours oxygen mobility affecting the redox behaviour of the material [37]. The calcination temperature also affects the

arrangement of atoms in the CeO_2 lattice (Figure 12a), and the intensity of the Raman peak increases with calcination temperature as a consequence of the better arrangement of atoms. Raman characterization also provides evidences of the improved thermal stability of the Ce-Zr mixed oxide. As shown on Figure 12b, the intensities of the signals of $Ce_{0.76}Zr_{0.24}O_2$ calcined between 500 and 900ºC are about the same, and increase slightly when calcined at 1000ºC. The shift of the Raman signal towards lower energies that occurs in $Ce_{0.76}Zr_{0.24}O_2$ calcined between 500 and 900ºC with regard to $Ce_{0.76}Zr_{0.24}O_2$-1000 is a sign of the improvement of oxygen mobility, which could be related to the presence of oxygen vacancies [38].

The redox properties of selected samples were investigated by H_2-TPR, and the H_2 consumption profiles obtained have been plotted on Figure 13. H_2 consumption must be attributed to the reduction of Ce^{4+} to Ce^{3+}, since Zr^{4+} is a non-reducible cation. It is generally accepted [39] that two peaks characterise the reduction profile of pure CeO_2. The first peak, centred at around 500 ºC in the profile of CeO_2-500, is attributed to the reduction of the uppermost layers of Ce^{4+} and the second peak, centred at 800 ºC, is originated by the reduction of the bulk. The H_2-consumption profile of $Ce_{0.76}Zr_{0.24}O_2$-500 also shows this shape, but the peak intensity ratio (surface/bulk reduction) is higher for the mixed oxide. This suggests enhanced oxygen mobility within the $Ce_{0.76}Zr_{0.24}O_2$ lattice in comparison with the bare CeO_2. On the other hand, a certain degree of inhomogeneous distribution of cerium and zirconium can be also inferred. A broad H_2-consumption band would be expected for a true Ce-Zr solid solution, where the surface and bulk reduction would occur concurrently, but not a clear distinction between surface and bulk reduction. Wu et al. [40] also reported a bimodal H_2-TPR profile for a $Ce_{0.5}Zr_{0.5}O_2$ sample which was ascribed to a possible "shell/core structure" concordant with a heterogeneous surface elemental

distribution. These authors reported a surface Ce/Zr ratio of 1.3, which is higher than the nominal ratio (1.0) for this sample. The results of XPS analysis performed with our $Ce_{0.76}Zr_{0.24}O_2$ mixed oxide also showed a Ce/Zr ratio of 5.0, well above the value of 3.2 expected for this nominal composition. On this line, Nagai et al [41,42] also assessed (by means of the XAFS technique) the existence of Ce- and Zr-rich domains in a $Ce_{0.5}Zr_{0.5}O_2$ solid solution prepared by co-precipitation and subsequent calcination at 500°C".

The profile of CeO_2-1000 only contains the bulk reduction peak due to the very low BET surface area of this sample. The drastic effect of the calcination temperature on the surface redox properties of CeO_2 is not so obvious in $Ce_{0.76}Zr_{0.24}O_2$. The H_2-consumption profile of $Ce_{0.76}Zr_{0.24}O_2$-1000 shows a broad band instead of two well-defined peaks, and the onset temperature of this band is consistent to a surface reduction process. The generally accepted suggestion to explain this type of profile is that the surface and bulk reduction occurs concurrently [39], that is, there is not a clear distinction between surface and bulk peaks because oxygen located within the bulk comes to the surface when surface oxygen is consumed. This type of profiles is characteristic of materials with good oxygen mobility.

As a summary, the characterization of CeO_2 and $Ce_{0.76}Zr_{0.24}O_2$ allows concluding that both materials present fluorite structure, and that Ce-Zr incorporates Zr^{4+} cations into the CeO_2 framework. This incorporation of foreign cations enhances the thermal resistance of CeO_2, diminishing thermal sintering. As a consequence of this improved thermal resistance, $Ce_{0.76}Zr_{0.24}O_2$ calcined at high temperature presents higher BET surface area and improved redox properties than pure CeO_2.

It is not easy to distinguish between the relative contribution of structural properties (BET area; particle size) and other properties like redox behaviour or lattice oxygen

mobility, in the catalytic activity towards soot combustion of CeO_2-based pure and mixed oxides. In order to get insight into this, the temperature for 50% soot conversion obtained from Temperature Programmed Reactions performed with the different CeO_2 and $Ce_{0.76}Zr_{0.24}O_2$ samples has been plotted as a function of their BET surface area on Figure 14. A relationship between both parameters is clearly observed, which allows concluding that the catalytic activity of pure CeO_2 and that of the mixed oxide $Ce_{0.76}Zr_{0.24}O_2$ depends on its surface area. A relationship between surface area and catalytic activity for soot oxidation in temperature programmed oxidations by O_2, with soot and catalyst in tight contact, has been also reported for the catalyst $Ce_{0.95}Fe_{0.05}O_{1.975}$ [19]. This catalyst was calcined at different temperatures in the range 500-750ºC, thus reaching surface areas in the range 92-10 m^2/g, respectively. A linear correlation between surface area and activity was obtained for surface areas below 40 m^2/g, while for larger area the variation in activity was not so relevant. In the present study, this threshold is not observed, probably because the soot and catalyst are in loose contact instead of tight. For experiments in loose contact, we also expect a threshold in surface area values above which the catalytic activity does not longer improves, but this limit seems to be above the maximum surface area reached in the current study ($67 m^2/g$).

In spite of the relationship between catalyst surface area and T50% values obtained in temperature programmed reactions (Figure 14), the isothermal reactions performed at 500ºC indicated that $Ce_{0.76}Zr_{0.24}O_2$-500 presents better activity than CeO_2-500 (and both samples present the same BET area). These differences could be explained by the improved redox properties, deduced from H_2-TPR (Figure 13), and/or enhanced lattice oxygen mobility, deduced from Raman spectroscopy (Figure 12), of the mixed oxide. In conclusion, the structural properties of CeO_2-based pure and mixed oxides play an

important role on their catalytic activity for soot oxidation but other properties like redox behaviour and/or enhanced lattice oxygen mobility, also affect their performance.

4.- Conclusions.

As a summary of the current study, it can be concluded that the catalytic activity of CeO_2 for Diesel-exhaust purification can be significantly improved by doping CeO_2 with Zr^{4+}, $Ce_{0.76}Zr_{0.24}O_2$ being the best formulation among those prepared and tested. This Ce-Zr mixed oxide presents a slightly higher activity than bare CeO_2 for soot oxidation by NO_x/O_2 when both catalysts are calcined at 500ºC (soot oxidation rates at 500ºC are 14.9 and 11.4 $\mu g_{soot}/s$, respectively), and both catalysts presents the same selectivity for CO_2 formation as soot oxidation product. However, $Ce_{0.76}Zr_{0.24}O_2$ shows enhanced thermal stability in comparison to pure CeO_2 (as deduced form XRD, Raman, TEM, N_2 adsorption and H_2-TPR characterization), maintaining part of its activity for soot oxidation and selectivity towards CO_2 formation after calcination at temperatures as high as 1000ºC.

In addition, $Ce_{0.76}Zr_{0.24}O_2$ catalyses more efficiently than CeO_2 the reduction of NO_x by soot around 500ºC, therefore contributing to the decrease of the NO_x emission level.

The catalytic activity of CeO_2 and $Ce_{0.76}Zr_{0.24}O_2$ for soot oxidation by NO_x/O_2 depends on their textural properties (BET area; crystallite size), but other properties of the oxides, like redox behaviour and/or enhanced lattice oxygen mobility, also play a significant role.

Acknowledgements

The authors thank the financial support of the project CTQ2005-01358 of the Spanish Ministry of Education and Science and ABL the contract funded by the Ramon y Cajal Program and the Generalidat Valenciana.

Literature

[1] M. V. Twigg, Appl. Catal. B 70 (2007) 2.

[2] J. Kašpar, P. Fornasiero, M. Graziani, Catal. Today 50 (1999) 285.

[3] A. Trovarelli. "Catalysis by Ceria and Related Materials". Catalytic Science Series, Vol. 2, Imperial College Press, p. 281 (2002).

[4] H.S. Gandhi, G.W. Graham, R.W. McCabe, J. Catal. 216 (2003) 433.

[5] P. Fornasiero, G. Balducci, J. Kašpar, S. Meriani, R. di Monte, M. Graziani. Catal. Today 29 (1996) 47.

[6] C. E. Hori, H. Permanaa, K.Y. Simon Ng, A. Brenner, K. More, K. M. Rahmoellerd, D. Belton, Appl.Catal. B 16 (1998) 105.

[7] M. Daturi, E. Finocchio, C. Binet, J.C. Lavalley, F. Fally, V. Perrichon, H. Vidal, N. Hickey, J. Kašpar. J. Phys. Chem. B 104 (2000) 9186.

[8] N. Hickey, P. Fornasiero, J. Kašpar, J. M. Gatica, S. Bernal. J. Catal. 200 (2001) 181.

[9] G. Balducci, J. Kašpar, P. Fornasiero, M. Graziani, M. Saiful Islam, J. Phys. Chem. B 102 (1998) 557.

[10] B.M. Reddy, P. Lakshmanan, P. Bharali, P. Saikia, G. Thrimurthulu, M. Muhler, W. Gru1nert, J. Phys. Chem. C 111 (2007) 10478.

[11] S. Eriksson, S. Rojas, M. Boutonnet, J.L.G. Fierro, Appl. Catal. A 326 (2007) 8.

[12] D. Terribile, A. Trovarelli, C. de Leitenburg, A. Primavera, G. Dolcetti, Catal. Today 47 (1999) 133.

[13] J. I. Gutiérrez-Ortiz, B. de Rivas, R. López-Fonseca, J. R. González-Velasco, Appl. Catal. B 65 (2006) 191.

[14] F. Fally, V. Perrichon, H. Vidal, J. Kašpar, G. Blanco, J.M. Pintado, S. Bernal, G. Colon, M. Daturi, J.C. Lavalley, Catal. Today 59 (2000) 373.

[15] I. Atribak, A. Bueno-López, A. García-García, Catal. Commun. 9 (2008) 250.

[16] A. Bueno-López, K. Krishna, M. Makkee, J. A. Moulijn, Catal. Letters 99 (2005) 203.

[17] B. A. A. L. van Setten, M. Makkee, J. A. Moulijn, Catal. Rev. 43 (2001) 489.

[18] J. P.A. Neeft, M. Makkee, J. A. Moulijn, Fuel. Proc. Technol. 47 (1996) 1.

[19] E. Aneggi, C. de Leitenburg, G. Dolcetti, A. Trovarelli, Catal. Today 114 (2006) 40.

[20] A. Bueno-López, K. Krishna, M. Makkee, J.A. Moulijn, J. Catal. 230 (2005) 237.

[21] K. Krishna, A. Bueno-López, M. Makkee, J.A. Moulijn, Appl. Catal. B 75 (2007) 189.

[22] I. Atribak, I. Such-Basáñez, A. Bueno-López, A. García García, J. Catal. 250 (2007) 75.

[23] A. Setiabudi, J.Chen, G. Mul, M. Makkee, J. A. Moulijn, Appl. Catal. B 51 (2004) 9.

[24] K. Krishna, A. Bueno-López, M. Makkee, J.A. Moulijn, Appl. Catal. B 75 (2007) 201.

[25] K. Krishna, A. Bueno-López, M. Makkee, J.A. Moulijn, Appl. Catal. B 75 (2007) 210.

[26] M.L. Pisarello, V. Milt, M.A. Peralta, C.A. Querini, E.E. Miró, Catal. Today 75 (2002) 465.

[27] B.A.A.L. van Setten, J.M. Schouten, M. Makkee, J.A. Moulijn, Appl. Catal. B 28 (2000) 253.

[28] M. Adamowska, S. Muller, P. Da Costa, A. Krzton, P. Burg, Appl. Catal. B 74 (2007) 278.

[29] M. Pijolat, M. Prin, M. Soustelle, O. Touret, P. Nortier, J. Chem. Soc. Faraday Trans. 91 (1995) 3941.

[30] A. Setiabudi, M. Makkee, J. A. Moulijn. Appl. Catal. B 50 (2004) 185.

[31] A. Bueno-López, A. García-García, J.A. Caballero-Suárez, Environ. Sci. Technol. 36 (2002) 5447.

[32] A. Bueno-López, A. García-García, A. Linares-Solano, Fuel Proc. Technol. 77–78 (2002) 301.

[33] D. Terribile, A. Trovarelli, J. Llorca, C. de Leitenburg, G. Dolcetti, Catal. Today 43 (1998) 79.

[34] A. Nineshige, T. Taji, Y. Muroi, M. Kobune, S. Fujii, N. Nishi, M. Inaba, Z. Ogumi, Solid State Ionics 135 (2000) 481.

[35] L.N. Ikryannikova, A.A. Aksenov, G.L. Markayan, G.P. Muravieva, B.G. Kostyuk, A.N. Kharlanov, E.V. Linina, Appl. Catal. A 210 (2001) 225.

[36] M. Fernandez-García, A. Martínez-Arias, A. Iglesias-Juez, C. Belver, A.B. Hungría, J.C. Conesa, J. Soria, J. Catal. 194 (2000) 385.

[37] P. Fornasiero, J. Kašpar, M. Grazini, J. Catal. 167 (1997) 576.

[38] S. Rossignol, C. Descorme, C. Kappenstein, D. Duprez, J. Mater. Chem. 11 (2001) 2587.

[39] G.L. Markaryan, L.N. Ikryannikova, G.P. Muravieva, A.O. Turakulova, B.G. Kostyuk, E.V. Lunina, V.V. Lunin, E. Zhilinskaya, A. Aboukais, Colloids Surfaces A 151 (1999) 435.

[40] W. Xiadong, L. Qing, W. Xiaodi, W. Duan, J. Rare Earths 25 (2007) 416.

[41] Y. Nagai, T. Yamamoto, T. Tanaka, S. Yoshida, T. Nonaka, T. Okamoto, A. Suda, M. Sugiura, J. Synchrotron Rad. 8 (2001) 616.

[42] Y. Nagai, T. Yamamoto, T. Tanaka, S. Yoshida, T. Nonaka, T. Okamoto, A. Suda, M. Sugiura, Catal. Today 74 (2002) 225.

FIGURE CAPTIONS

Figure 1. Effect of the Ce:Zr ratio on soot combustion.

Figure 2. Effect of the Ce:Zr ratio on CO emission.

Figure 3. Effect of the calcination temperature of catalyst on soot combustion.

Figure 4. Effect of the calcination temperature of catalyst on CO emission.

Figure 5. Effect of the Ce:Zr ratio on: (a) NO_x elimination and (b) O_2 elimination (catalysts calcined at 500ºC).

Figure 6. Blank experiments (without soot): (a) NO_x elimination and (b) NO_2 formation.

Figure 7. Effect of the calcination temperature of catalyst on NO_x elimination: (a) CeO_2-series and (b) $Ce_{0.76}Zr_{0.24}O_2$-series.

Figure 8. Isothermal reactions at 500ºC: (a) soot oxidation rate and (b) NO_x elimination. (The units of soot oxidation rate are mg of soot converted per second and gram of soot remaining in the reactor)

Figure 9. BET surface areas in terms of calcination temperature of catalysts.

Figure 10. TEM images : a) CeO_2-500, b) CeO_2-1000, c) $Ce_{0.76}Zr_{0.24}O_2$-500, d) $Ce_{0.76}Zr_{0.24}O_2$-1000.

Figure 11. XRD characterisation of catalysts: (a) CeO_2-series and (b) $Ce_{0.76}Zr_{0.24}O_2$-series.

Figure 12. Raman characterisation of catalysts: (a) CeO_2-series and (b) $Ce_{0.76}Zr_{0.24}O_2$-series.

Figure 13. H_2 consumption profiles during H_2-TPR for selected catalysts.

Figura 14. T50% parameter versus BET surface area of catalysts (CeO_2-series and $Ce_{0.76}Zr_{0.24}O_2$-series).

Table 1. Data estimated from isothermal reactions at 500ºC.

Catalyst	CO/CO_x (%)	Time for 75% soot conversion (min)	Average soot oxidation rate ($\mu g_{soot}/s$)
CeO_2-500	2.1	24	11.4
CeO_2-1000	11.3	172	1.2
$Ce_{0.76}Zr_{0.24}O_2$-500	3.5	19	14.9
$Ce_{0.76}Zr_{0.24}O_2$-1000	36.8	62	4.1

Table 2. Crystal sizes determined from XRD.

	Crystal size (nm) with Williamson-Hall's equation	Crystal size (nm) with Scherrer's equation
CeO_2-500	22	14
CeO_2-600	22	19
CeO_2-700	46	32
CeO_2-800	63	38
CeO_2-900	116	58
CeO_2-1000	107	55
$Ce_{0.76}Zr_{0.24}O_2$-500	10	11
$Ce_{0.76}Zr_{0.24}O_2$-600	21	13
$Ce_{0.76}Zr_{0.24}O_2$-700	20	9
$Ce_{0.76}Zr_{0.24}O_2$-800	17	12
$Ce_{0.76}Zr_{0.24}O_2$-900	19	13
$Ce_{0.76}Zr_{0.24}O_2$-1000	65	22

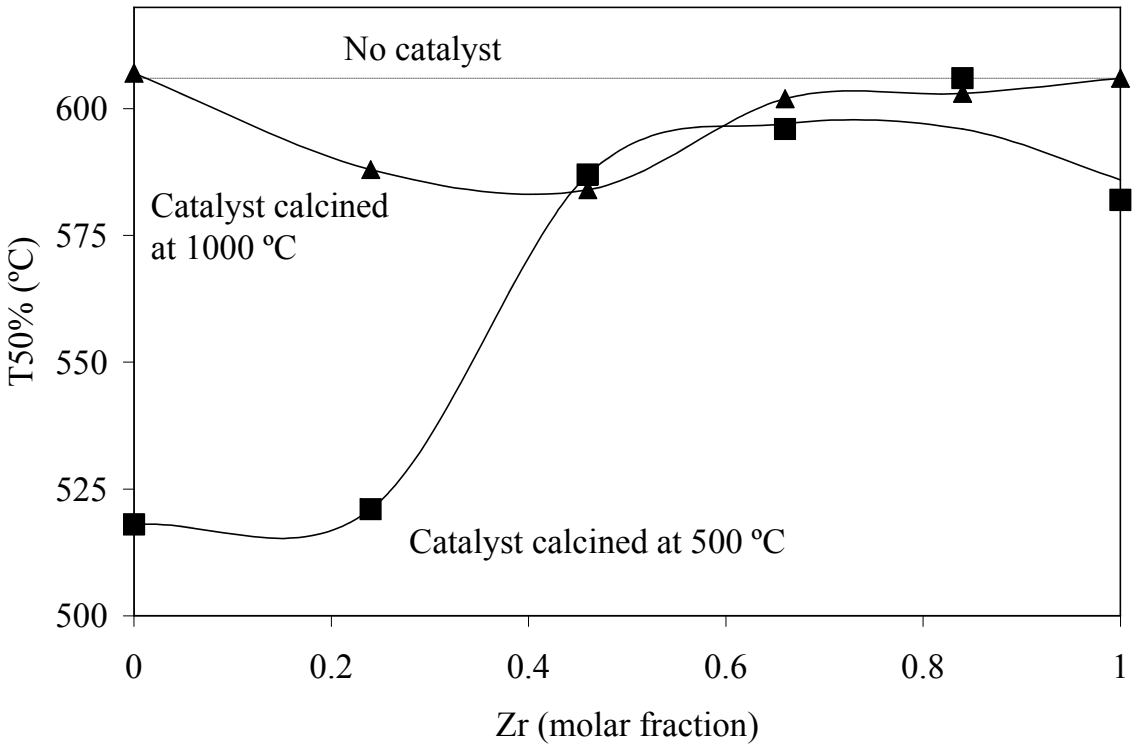
No catalyst
Catalyst calcined
at 1000 ºC
Catalyst calcined at 500 ºC
T50% (ºC)
600
575
550
525
500
0
0.2
0.4
0.6
0.8
1
Zr (molar fraction)

Figure 1

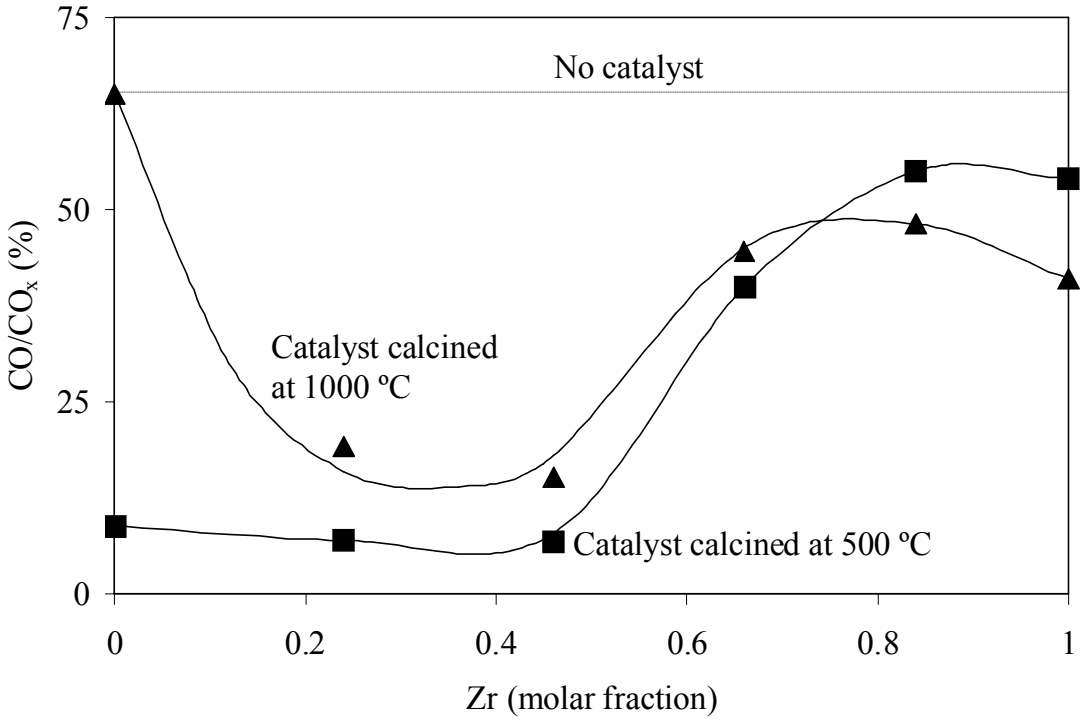
75
50
25
0
No catalyst
Catalyst calcined
at 1000 ºC
Catalyst calcined at 500 ºC
CO/CO$_x$ (%)
0
0.2
0.4
0.6
0.8
1
Zr (molar fraction)

Figure 2

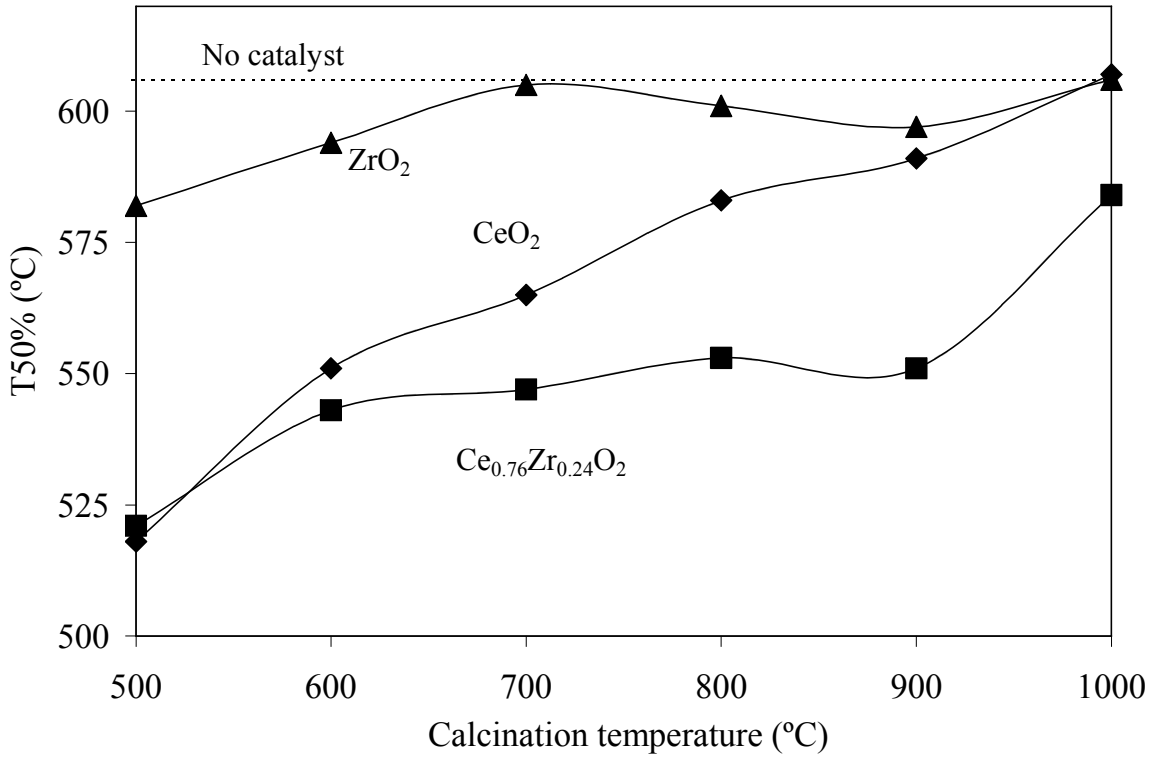
No catalyst
600
575
550
525
500
T50% (ºC)
ZrO2
CeO2
Ce0.76Zr0.24O2
500
600
700
800
900
1000
Calcination temperature (ºC)

Figure 3

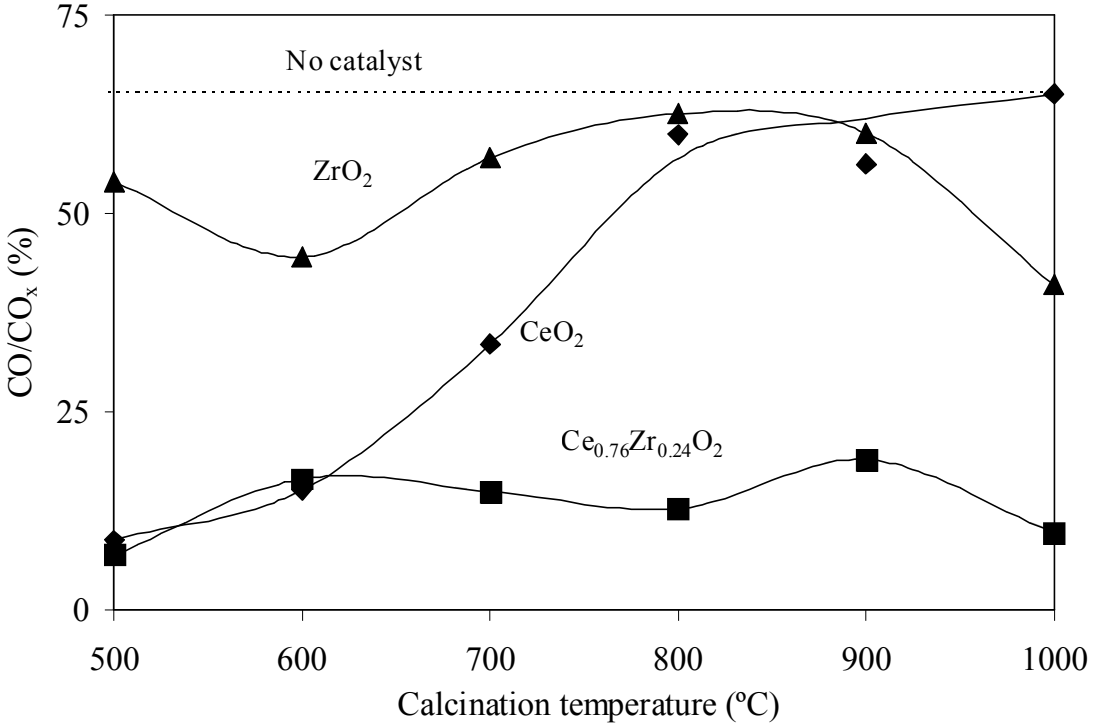
75
50
25
0
No catalyst
ZrO_2
CeO_2
$Ce_{0.76}Zr_{0.24}O_2$
CO/CO_x (%)
500
600
700
800
900
1000
Calcination temperature (ºC)

Figure 4

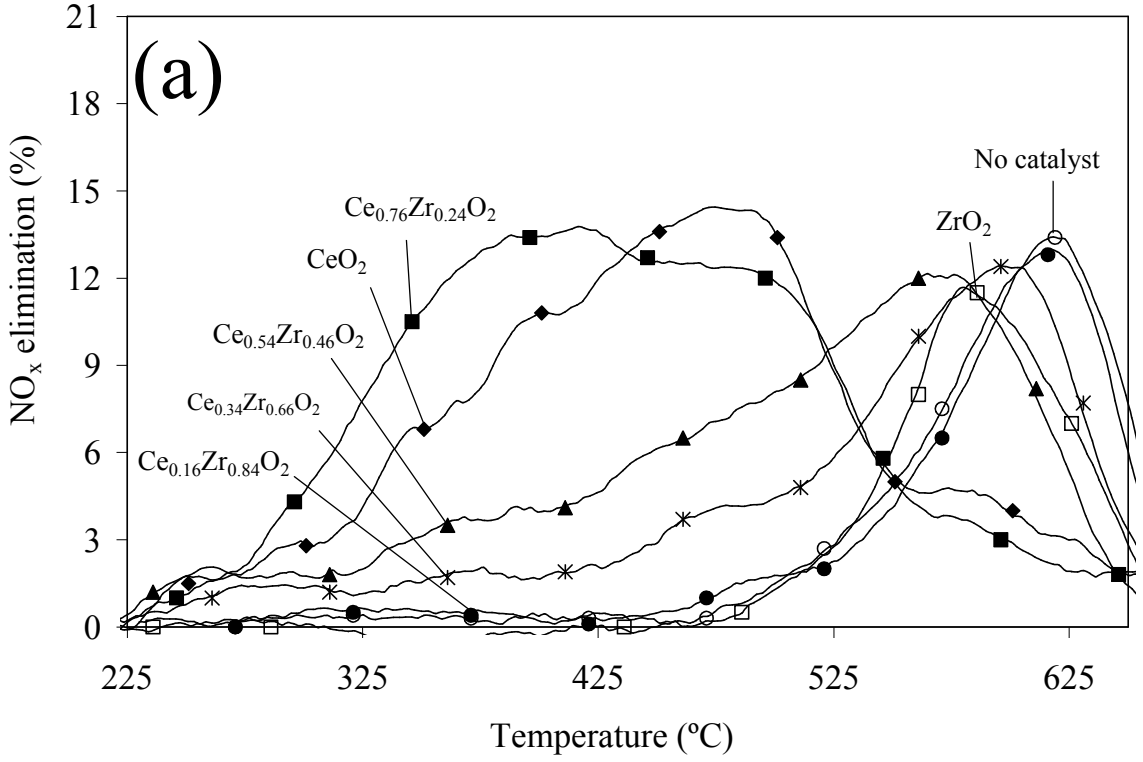
(a)
NOx elimination (%)
Temperature (ºC)
Ce0.76Zr0.24O2
CeO2
Ce0.54Zr0.46O2
Ce0.34Zr0.66O2
Ce0.16Zr0.84O2
ZrO2
No catalyst

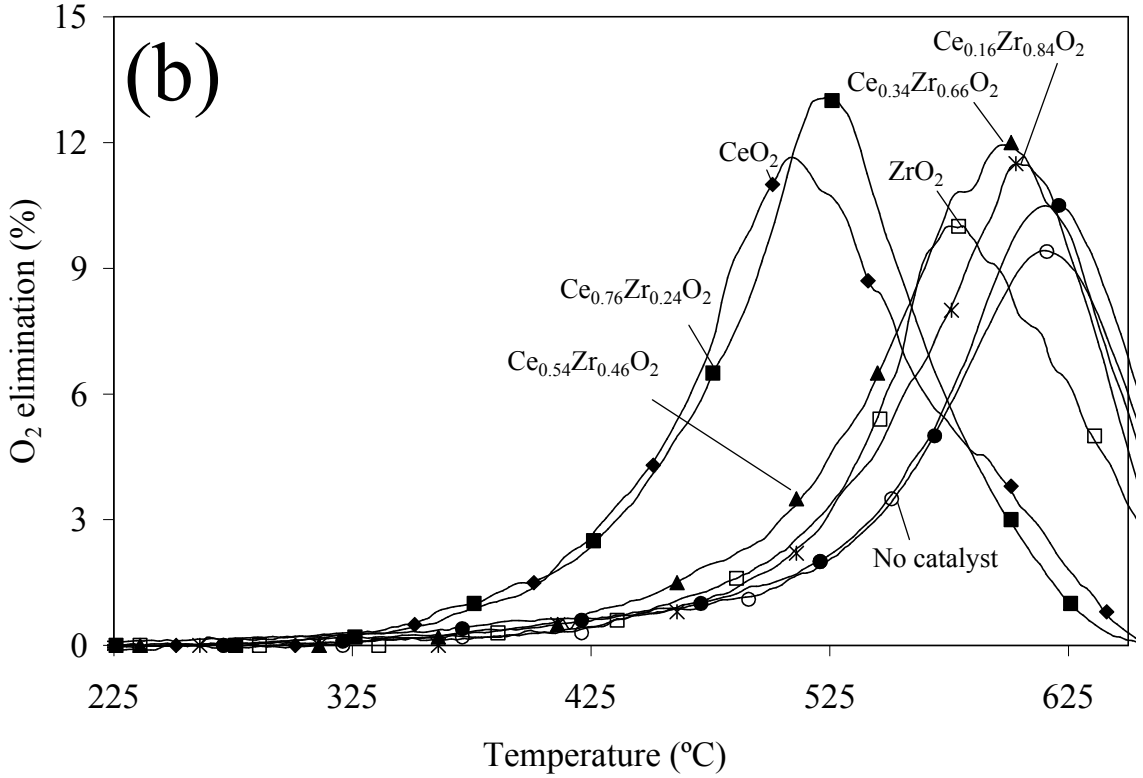
(b)
O2 elimination (%)
Temperature (ºC)
Ce0.16Zr0.84O2
Ce0.34Zr0.66O2
CeO2
ZrO2
Ce0.76Zr0.24O2
Ce0.54Zr0.46O2
No catalyst

Figure 5

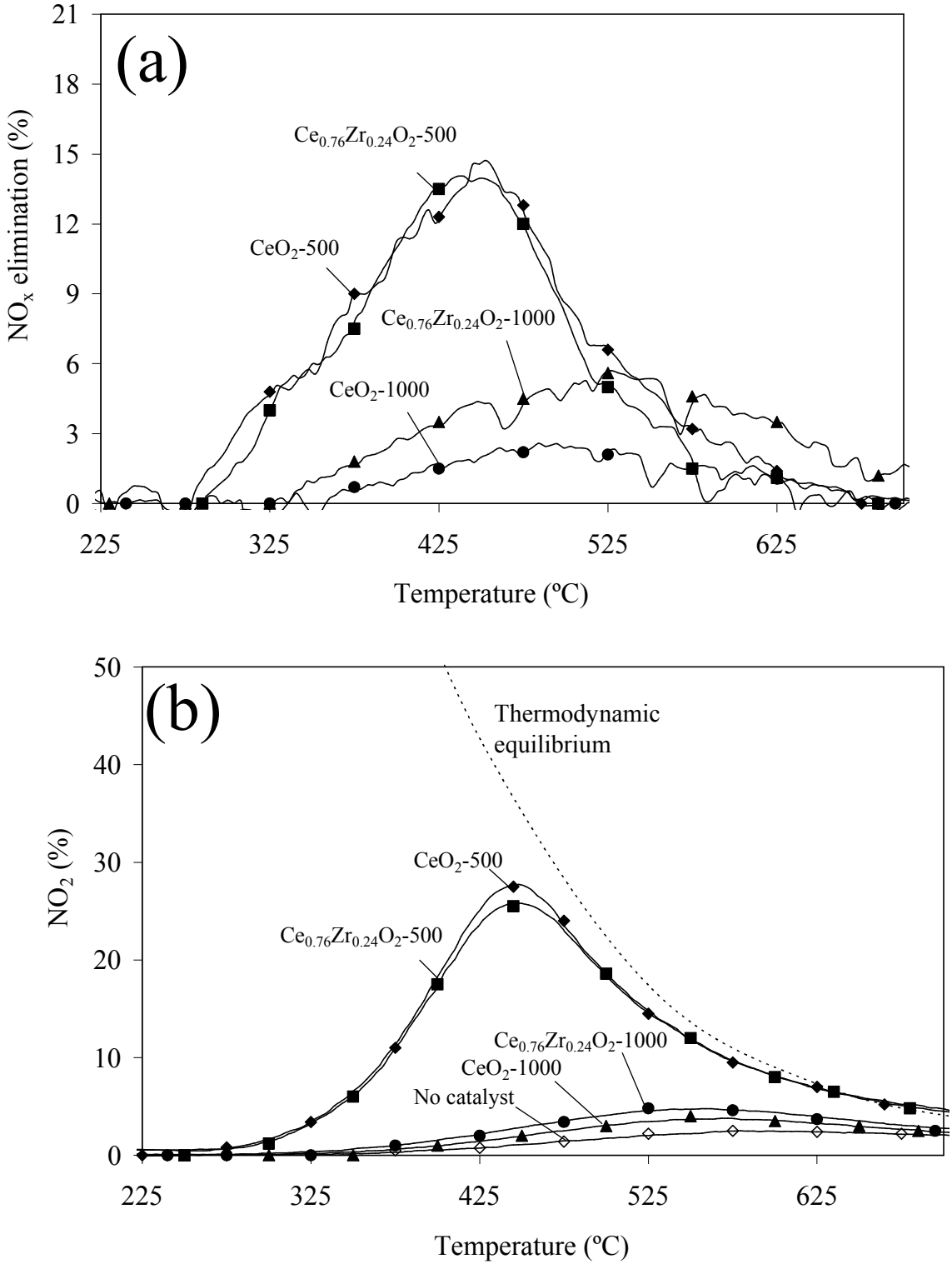
(a)
NO_x elimination (%)
21
18
15
12
9
6
3
0
225
325
425
525
625
Temperature (ºC)
$Ce_{0.76}Zr_{0.24}O_2$-500
CeO_2-500
$Ce_{0.76}Zr_{0.24}O_2$-1000
CeO_2-1000
(b)
NO_2 (%)
50
40
30
20
10
0
225
325
425
525
625
Temperature (ºC)
Thermodynamic equilibrium
CeO_2-500
$Ce_{0.76}Zr_{0.24}O_2$-500
$Ce_{0.76}Zr_{0.24}O_2$-1000
CeO_2-1000
No catalyst

Figure 6

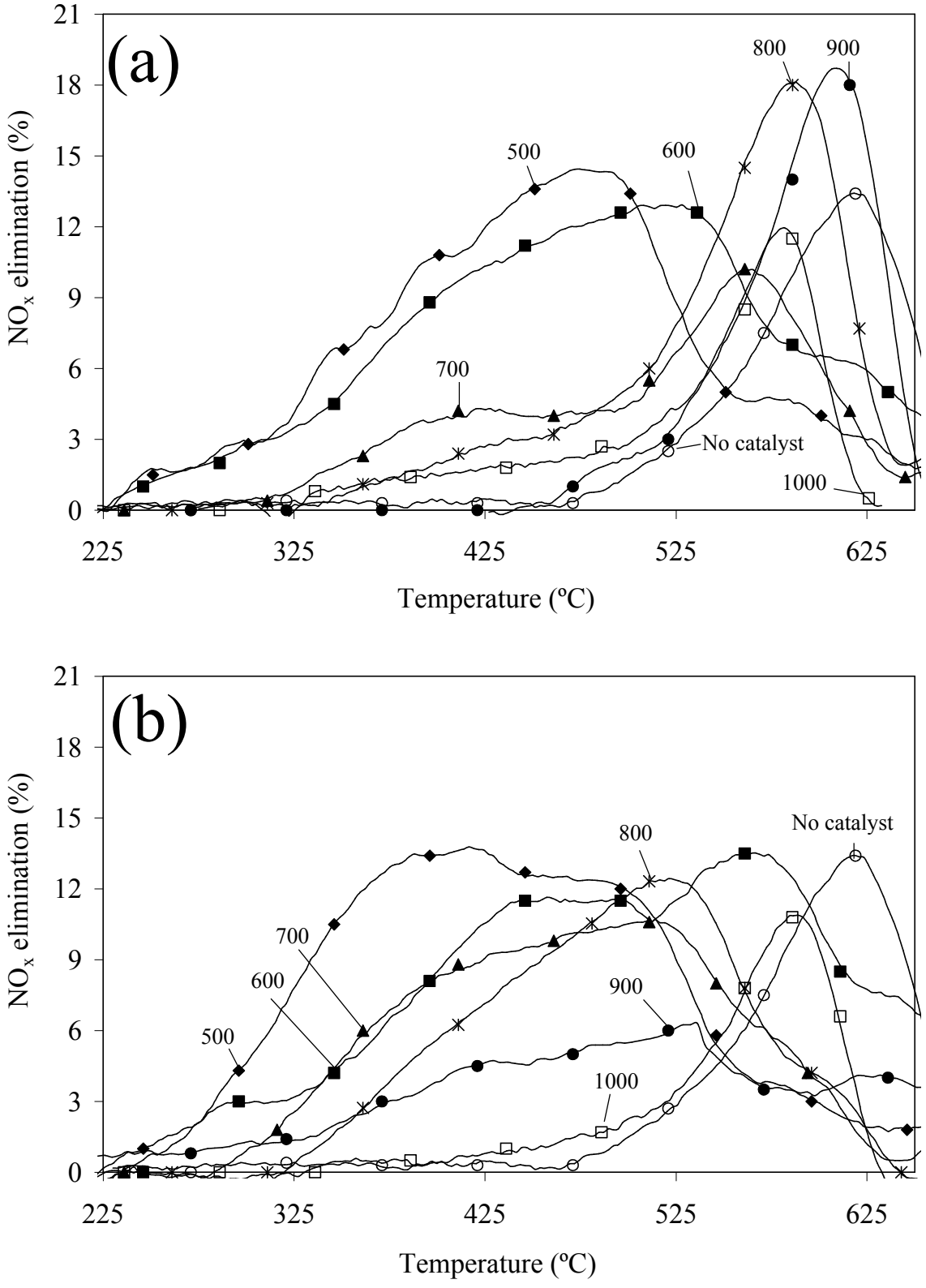
(a)
NO_x elimination (%)
Temperature (ºC)
500
600
700
800
900
1000
No catalyst
(b)
NO_x elimination (%)
Temperature (ºC)
500
600
700
800
900
1000
No catalyst

Figure 7

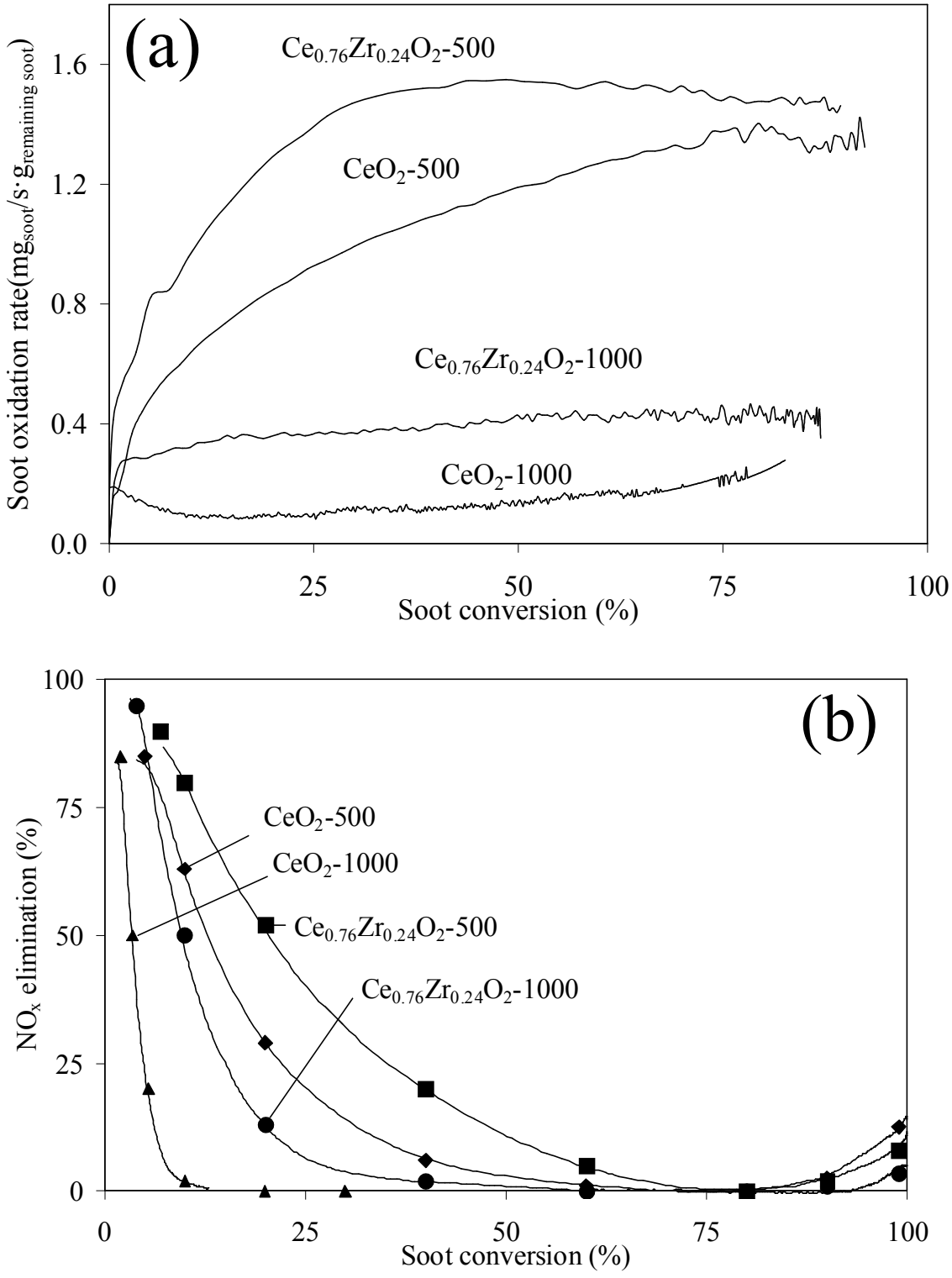
(a)
Ce0.76Zr0.24O2-500
CeO2-500
Ce0.76Zr0.24O2-1000
CeO2-1000
Soot oxidation rate(mgsoot/s·gremaining soot)
Soot conversion (%)
0.0
0.4
0.8
1.2
1.6
0
25
50
75
100
(b)
CeO2-500
CeO2-1000
Ce0.76Zr0.24O2-500
Ce0.76Zr0.24O2-1000
NOx elimination (%)
Soot conversion (%)
0
25
50
75
100

Figure 8

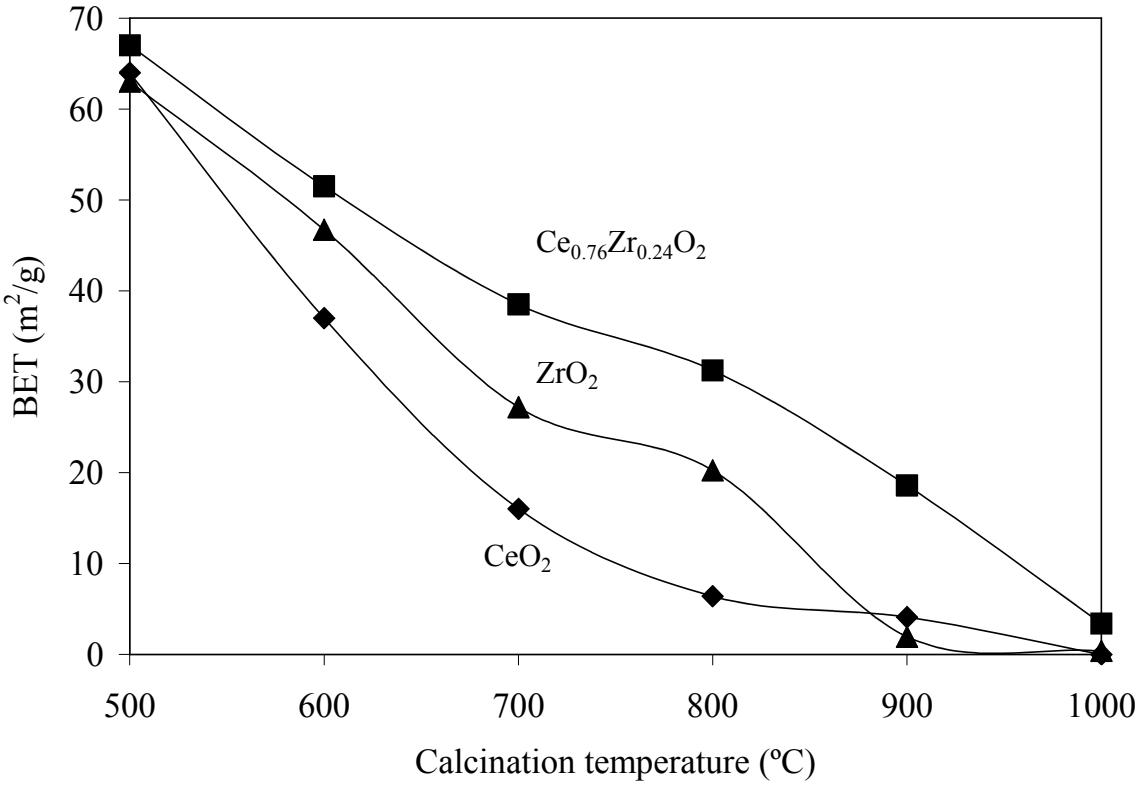
70
60
50
40
30
20
10
0
BET (m2/g)
Ce0.76Zr0.24O2
ZrO2
CeO2
500
600
700
800
900
1000
Calcination temperature (ºC)

Figure 9

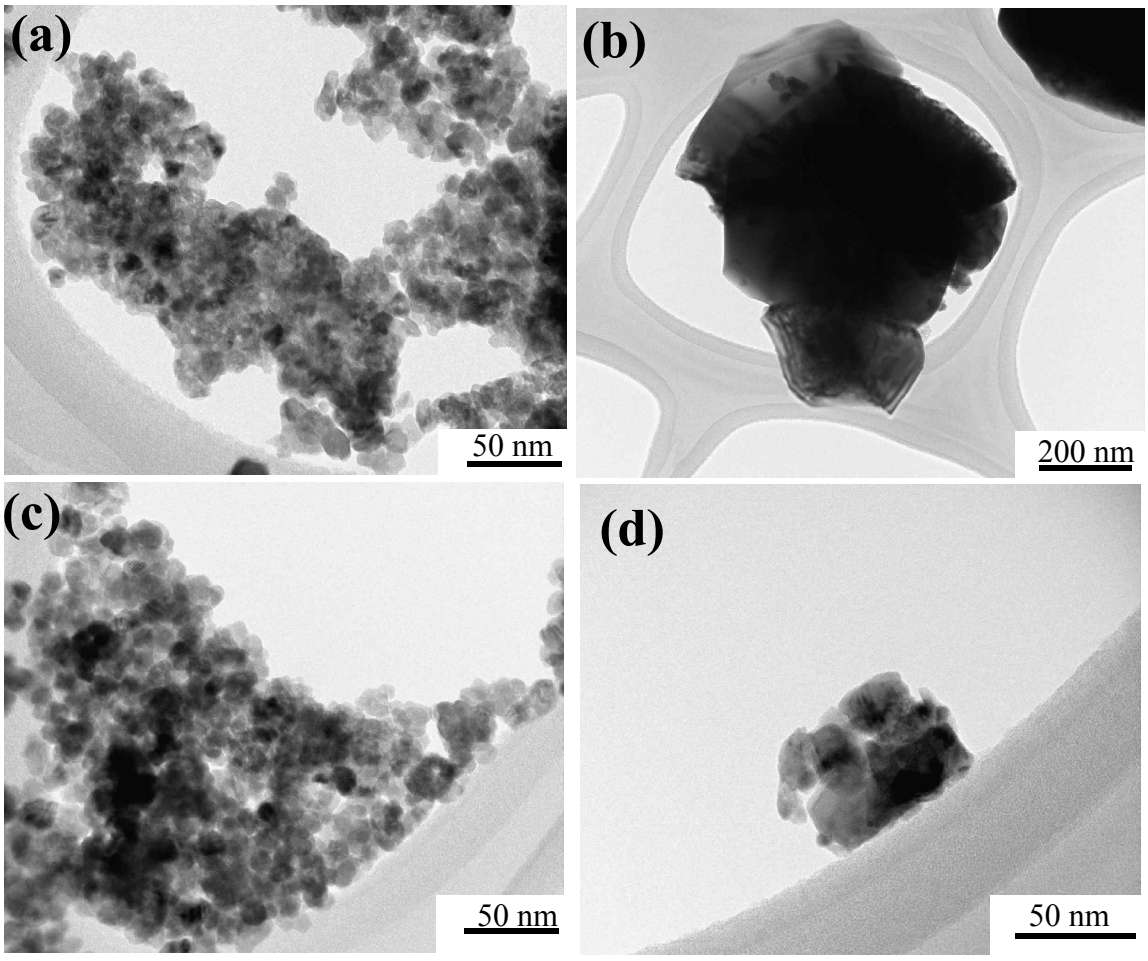

Figure 10

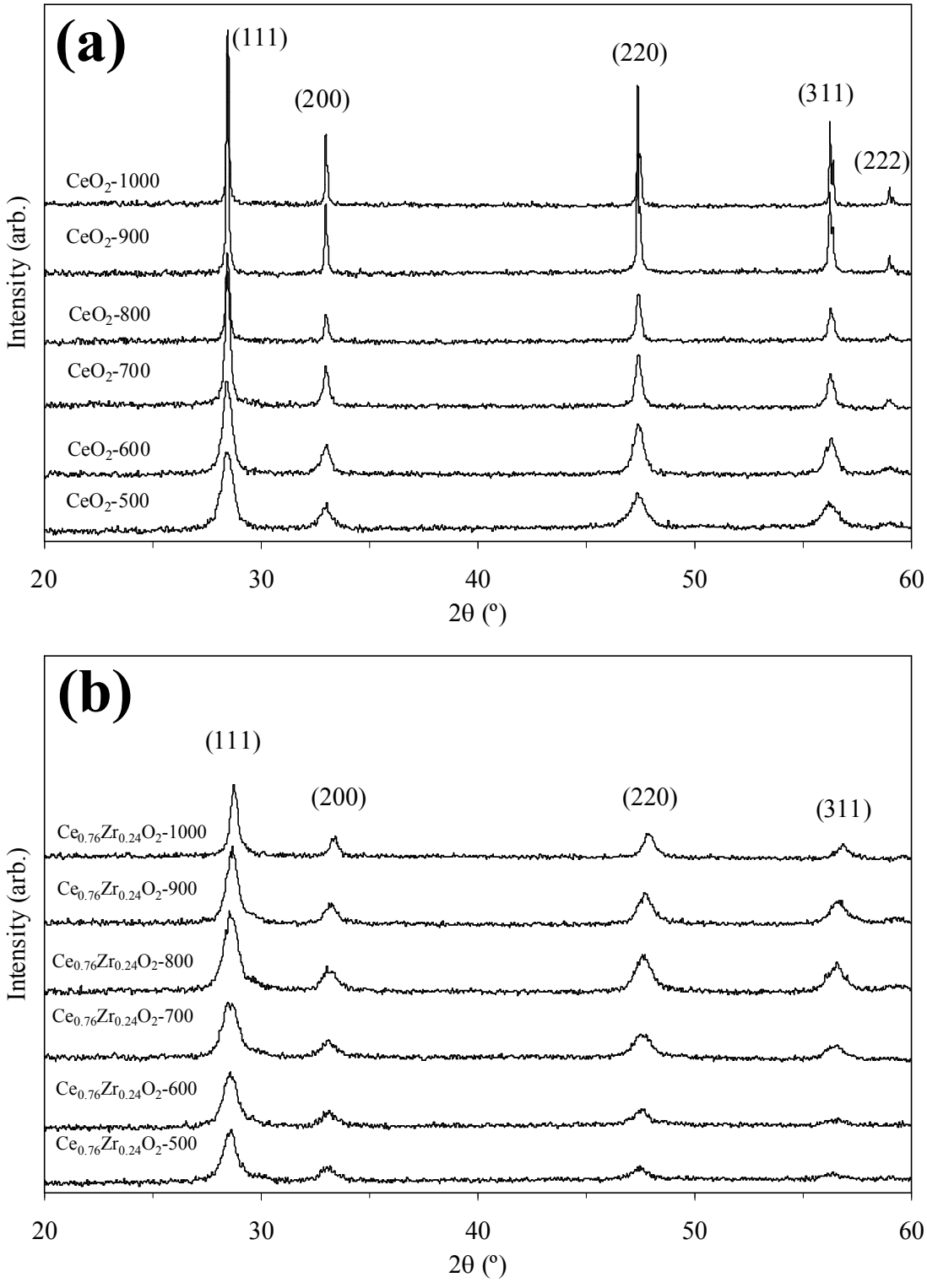
(a)
(111)
(200)
(220)
(311)
(222)
CeO2-1000
CeO2-900
CeO2-800
CeO2-700
CeO2-600
CeO2-500
Intensity (arb.)
20
30
40
50
60
2θ (º)
(b)
(111)
(200)
(220)
(311)
Ce0.76Zr0.24O2-1000
Ce0.76Zr0.24O2-900
Ce0.76Zr0.24O2-800
Ce0.76Zr0.24O2-700
Ce0.76Zr0.24O2-600
Ce0.76Zr0.24O2-500
Intensity (arb.)
20
30
40
50
60
2θ (º)

Figure 11

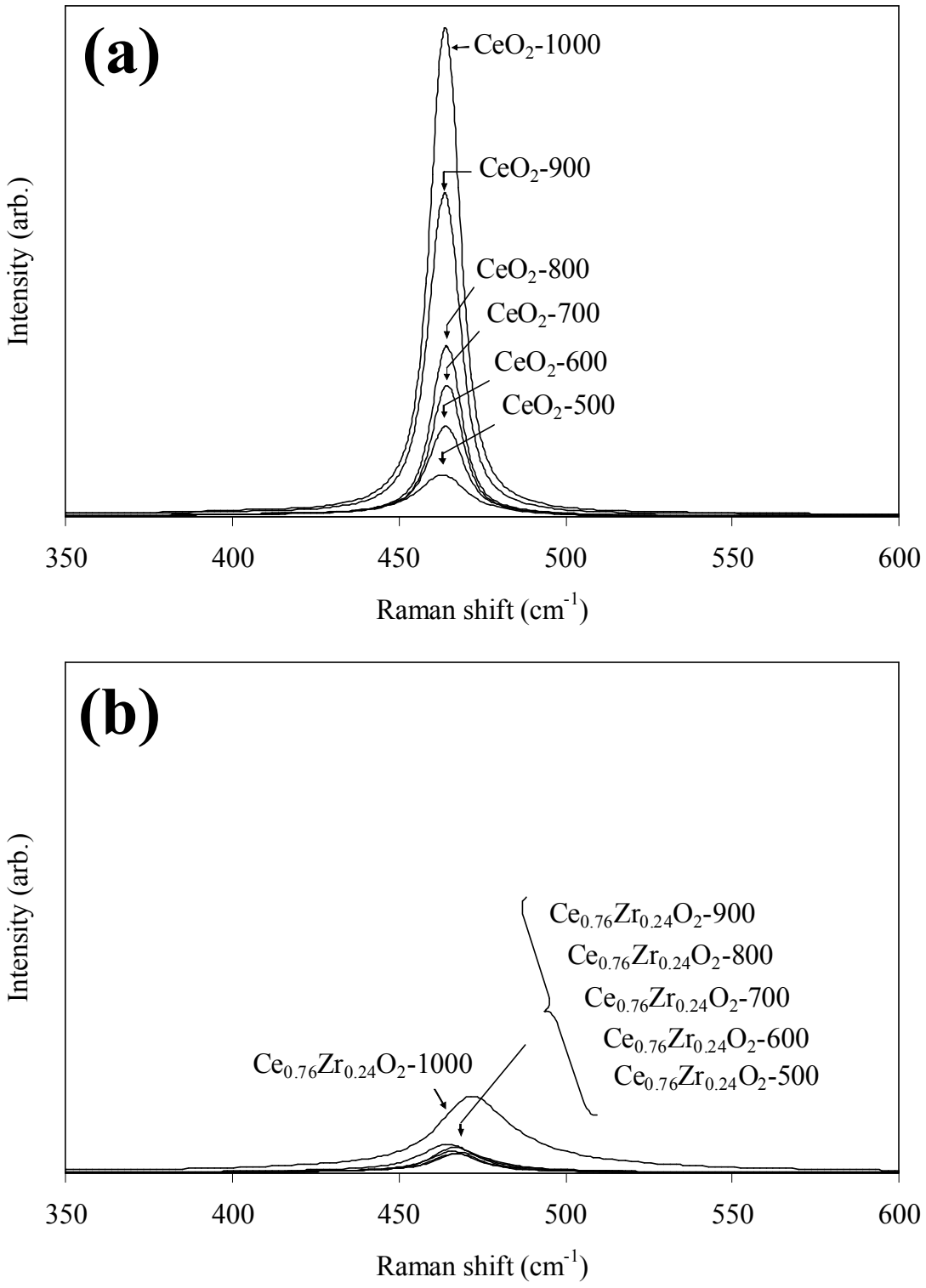
(a)
CeO2-1000
CeO2-900
CeO2-800
CeO2-700
CeO2-600
CeO2-500
Intensity (arb.)
350
400
450
500
550
600
Raman shift (cm-1)
(b)
Ce0.76Zr0.24O2-900
Ce0.76Zr0.24O2-800
Ce0.76Zr0.24O2-700
Ce0.76Zr0.24O2-600
Ce0.76Zr0.24O2-500
Ce0.76Zr0.24O2-1000
Intensity (arb.)
350
400
450
500
550
600
Raman shift (cm-1)

Figure 12

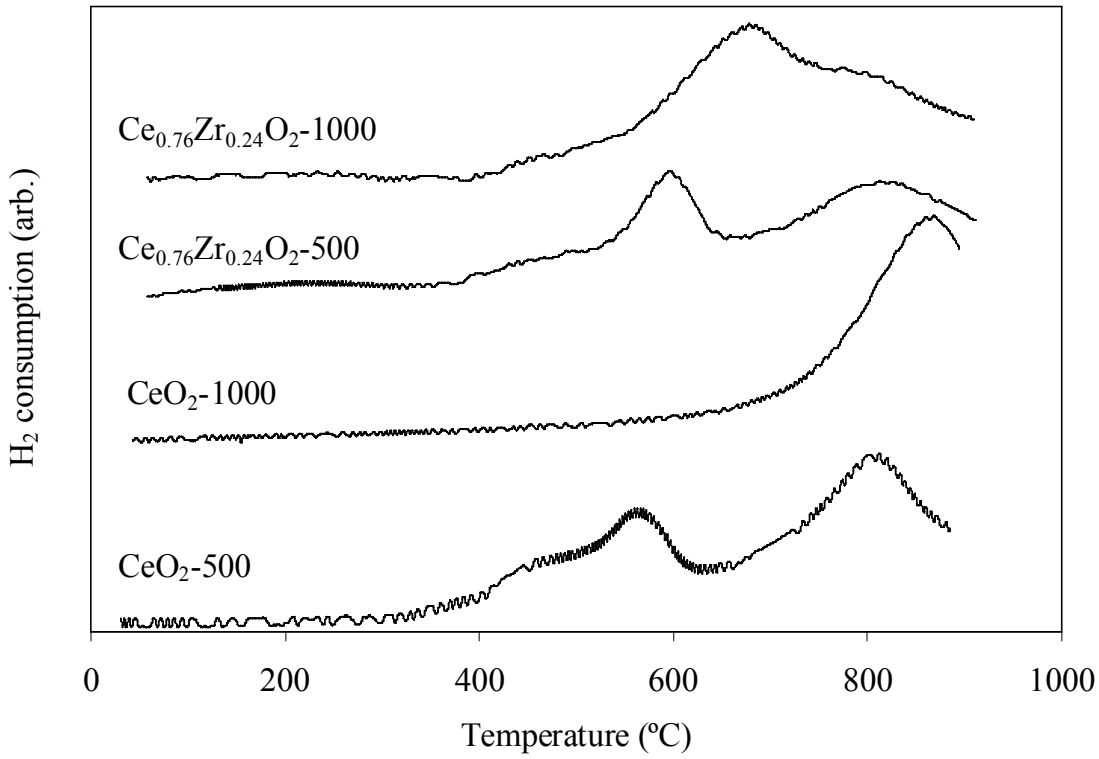
$Ce_{0.76}Zr_{0.24}O_2$-1000
$Ce_{0.76}Zr_{0.24}O_2$-500
CeO_2-1000
CeO_2-500
H_2 consumption (arb.)
0
200
400
600
800
1000
Temperature (ºC)

Figure 13

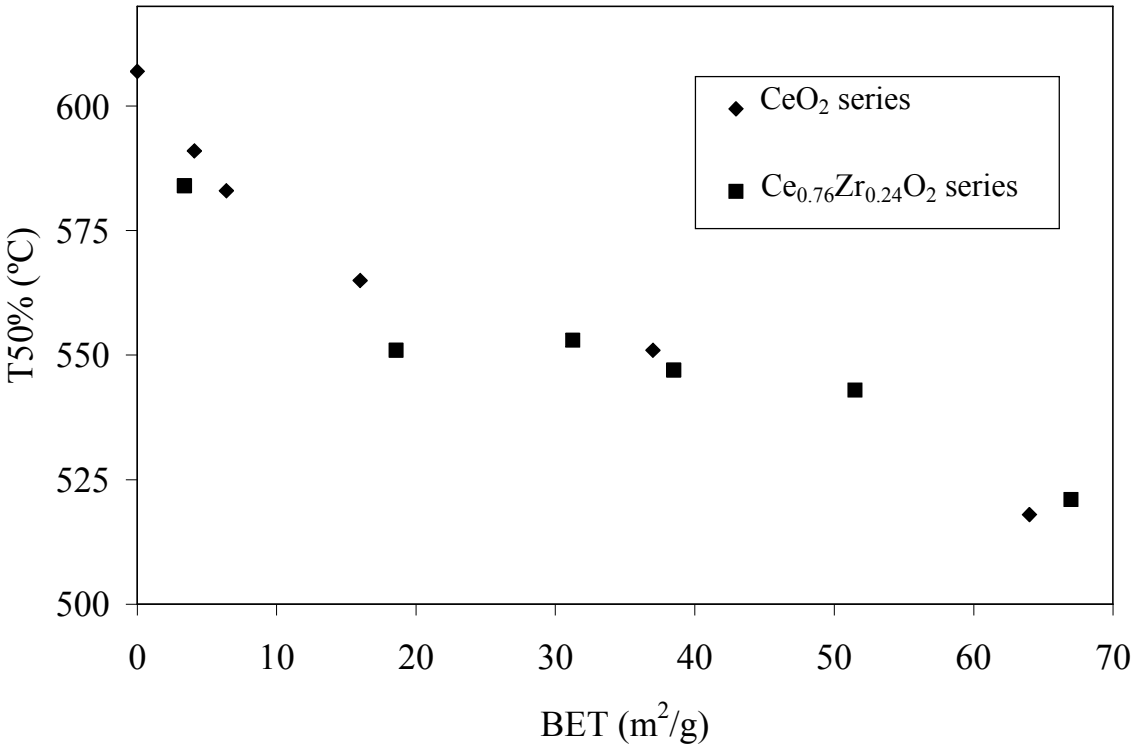
CeO2 series
Ce0.76Zr0.24O2 series
T50% (ºC)
600
575
550
525
500
0
10
20
30
40
50
60
70
BET (m2/g)

Figure 14